Supporting Information

Interfacial Reaction-Induced Defect Engineering: Enhanced Visible and Near-Infrared Absorption of Wide Band Gap Metal Oxides with Abundant Oxygen Vacancies

Fugong Qi, Zhenwen Yang, Jinfeng Zhang, Ying Wang, Qiwen Qiu, Huijun Li*

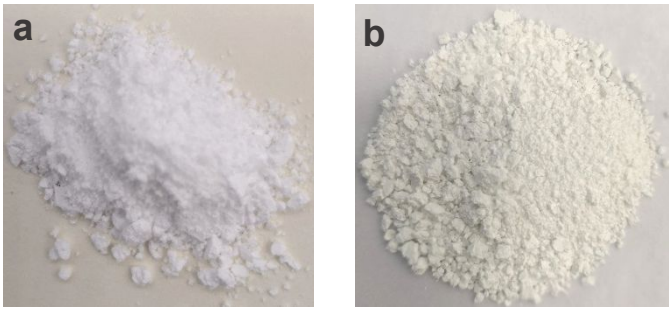

Figure S1. Pictures of a) pristine zirconia and b) the zirconia calcinated in vacuum at 1100 °C for 2h.

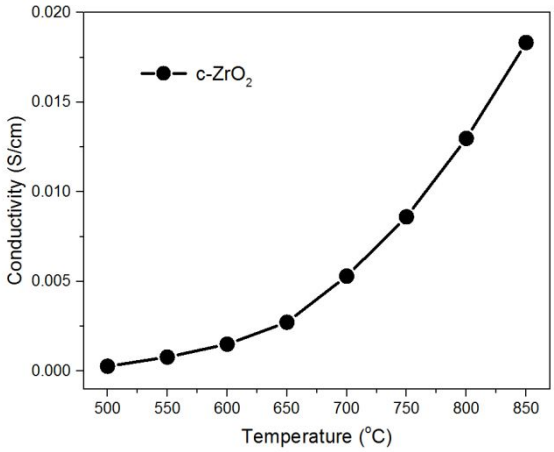

Figure S2. Conductivity of stabilized ZrO_2 at different temperatures.

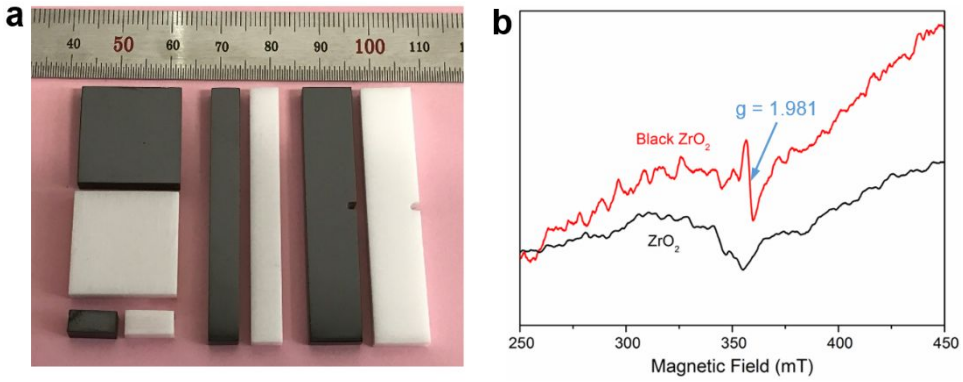

Figure S3. a) Pictures of prepared black ZrO_2 with different sizes at 1100 °C for 2h. b) Electron spin resonance spectra of bulk-sized ZrO_2. The pristine ZrO_2 (white) is ESR silent, while the black ZrO_2

has a distinct signal of structural defects.

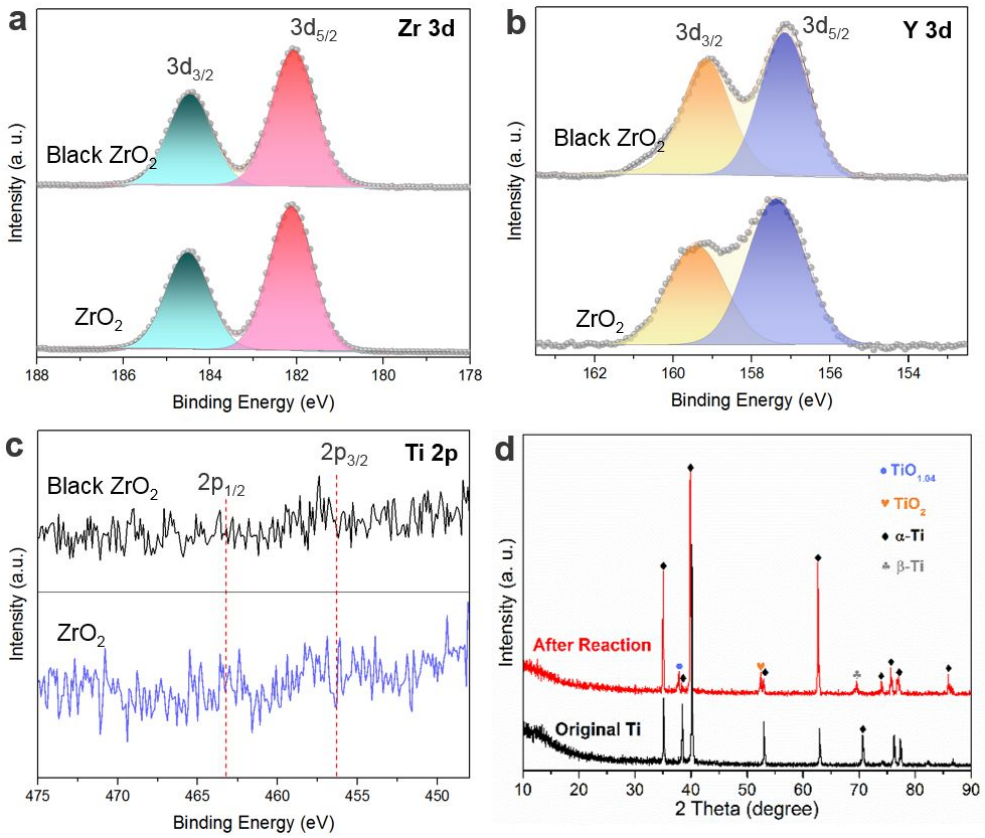

Figure S4. XPS spectra of a) Zr 3d, b) Y 3d, and c) Ti 2p core level peak regions of prepared samples, d) XRD of titanium component before and after the interfacial reaction.

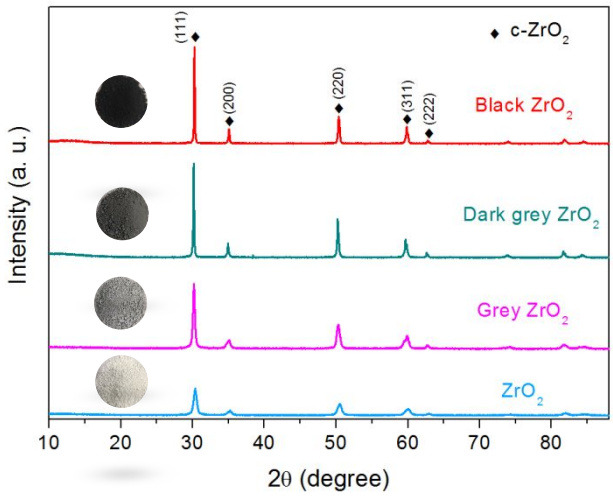

Figure S5. XRD patterns of modified and pristine ZrO_2. Black, dark grey, and grey ZrO_2 samples are prepared under 1100, 1000, and 900 ^oC respectively.

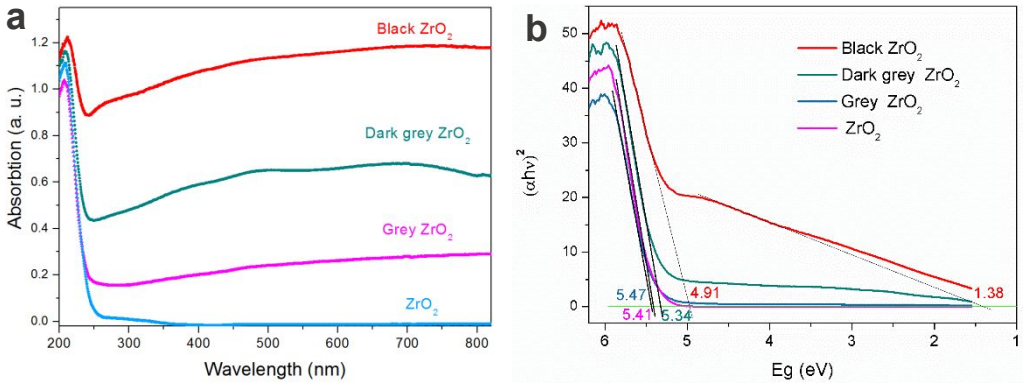

Figure S6. a) UV-VIS-NIR spectra and b) Tauc plots obtained from the UV-VIS-NIR data of prepared samples.

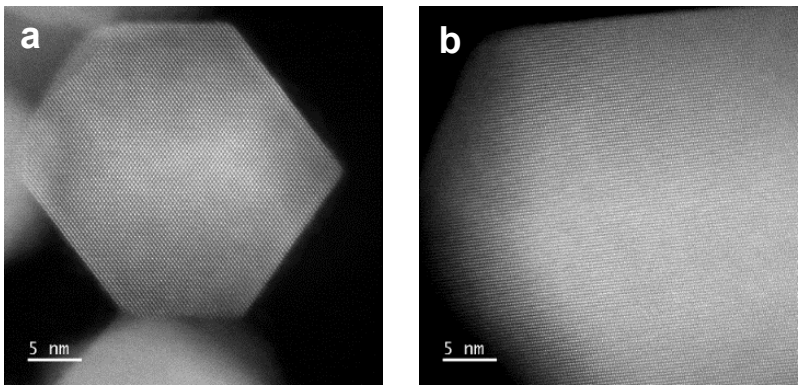

Figure S7. HADDF-STEM images of a) grey (900 °C) and b) dark grey (1000 °C) ZrO_2.

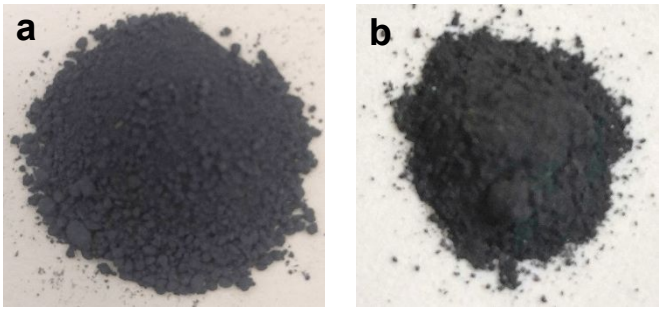

Figure S8. Pictures of a) initial prepared black zirconia and b) the black zirconia exposed in air for 100 days.

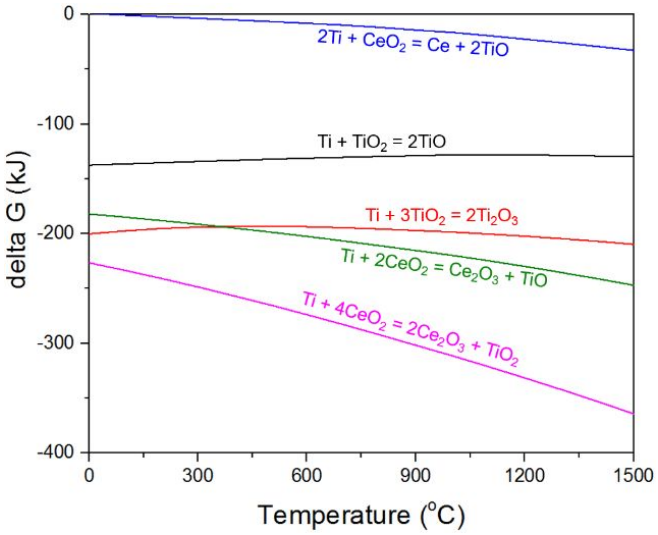

Figure S9. Gibbs free energy of the reaction between metallic Ti and metal oxide (TiO_2, CeO_2).

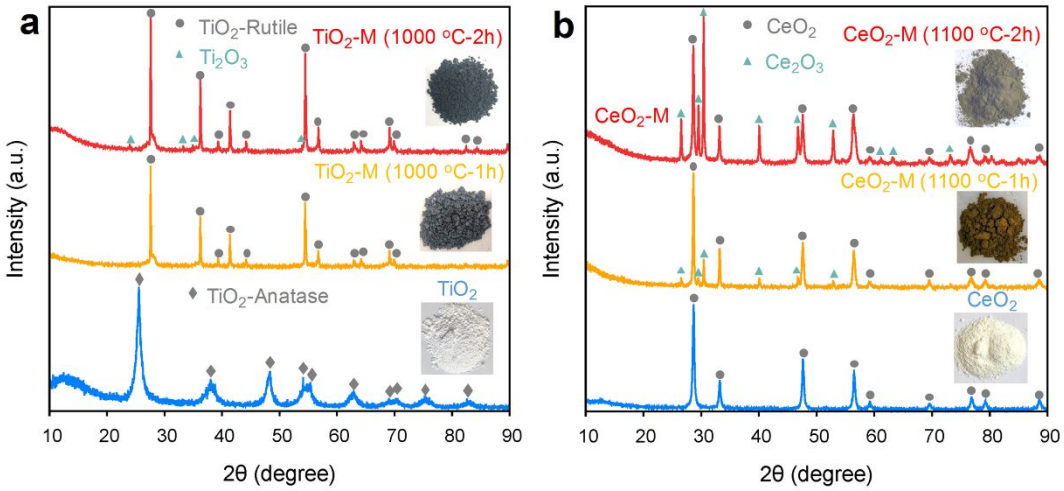

Figure S10. XRD patterns of pristine and modified a) TiO_2 and b) CeO_2 at different reaction conditions.

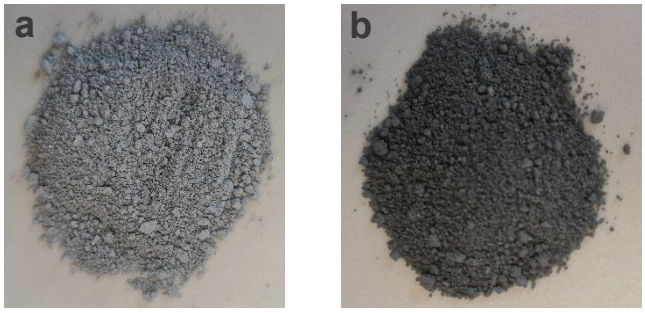

Figure S11 Pictures of modified a) m-ZrO_2 and b) c-ZrO_2 (YSZ) at 1100 °C for 1h. The modified c-ZrO_2 sample has a darker color than the modified m-ZrO_2 sample, which is attributed to the better

oxygen transport capacity of c-ZrO_2.

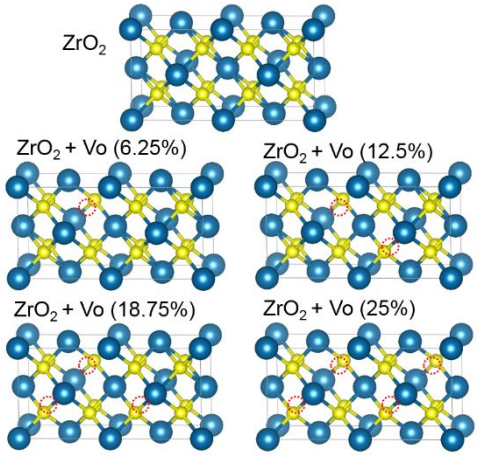

Figure S12. Calculated models with different oxygen vacancies concentration. Considering the good oxygen diffusion capacity of stabilized ZrO_2, the oxygen atoms tend to distribute uniformly, as well as the oxygen vacancies. In this case, the oxygen vacancies in these models were distributed as uniform as possible and there are no adjacent oxygen vacancies formed.

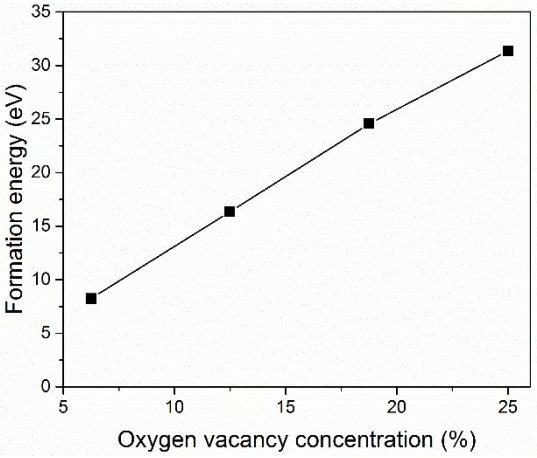

Figure S13 Formation energies of oxygen vacancy in ZrO_2 for different oxygen vacancy concentrations. The formation energy of oxygen vacancies was calculated by Equation (1).

$$E_f(\frac{n}{16}) = E_{Zr80(16-n)} + \frac{n}{2} * E_{O_2} - E_{Zr8016} \qquad (1)$$